Applied Catalysis B: Environmental 127 (2012) 330–335

Contents lists available at SciVerse ScienceDirect

Applied Catalysis B: Environmental

journal homepage: www.elsevier.com/locate/apcatb

Excellent performance of mesoporous Co_3O_4/MnO_2 nanoparticles in heterogeneous activation of peroxymonosulfate for phenol degradation in aqueous solutions

Hanwen Liang[a,b], Hongqi Sun[a], Archana Patel[c], Pradeep Shukla[c], Z.H. Zhu[c], Shaobin Wang[a,*]

[a] Department of Chemical Engineering, Curtin University, GPO Box U1987, Perth, WA 6845, Australia
[b] Department of Water Pollution Control Technology, Research Center for Eco-Environmental Sciences, Chinese Academy of Sciences, P.O. Box 2871, Beijing 100085, PR China
[c] School of Chemical Engineering, The University of Queensland, St. Lucia, QLD 4072, Australia

ARTICLE INFO

Article history:
Received 22 February 2012
Received in revised form 31 August 2012
Accepted 1 September 2012
Available online 7 September 2012

Keywords:
Mesoporous MnO_2
Supported Co oxide
Advanced oxidation
Water treatment
Nanorod particles

ABSTRACT

Mesoporous α-MnO_2 and its supported Co_3O_4 nanoparticles were synthesized, characterized and tested in heterogeneous activation of peroxymonosulfate (PMS) for phenol degradation in aqueous solution. α-MnO_2 supported Co_3O_4 presented as nanorod particles and showed H_2 redox reduction at low temperature. Bulk α-MnO_2 and Co_3O_4 could activate peroxymonosulfate to generate sulfate radicals for phenol degradation but at low activity. Co_3O_4/MnO_2 nanoparticles exhibited much high activity in peroxymonosulfate activation for phenol degradation with 100% conversion in 20 min and 3 wt% is the optimum Co loading. Phenol degradation followed a first order kinetics. Stability tests also showed that Co_3O_4/MnO_2 presented stable performance in phenol degradation in several runs.

1. Introduction

Organic pollutants are wide presence in wastewater from various sources including natural processes and industrial discharge. Most of organic compounds are toxic and detrimental to human health and the eco-environment. Degradation of organic pollutants in wastewater is one of the focuses in water treatment. Currently, many techniques have been developed for water treatment. One of them is advanced oxidation processes (AOPs), which use O_2, H_2O_2 or ozone to generate very reactive species, such as hydroxyl radicals ($OH^•$), to oxidize the pollutants quickly and efficiently [1–4].

Fenton reaction is the most popular way in advanced oxidation processes using homogeneous or heterogeneous Fe(II)/H_2O_2 systems. Apart from Fe, other metals can also be used in activation of H_2O_2, such as Mn or Cu. However, few studies have been conducted on the catalytic properties of manganese dioxide materials in water treatment and the ability of soluble manganese and manganese oxides to catalyze modified Fenton's reactions has not been studied in depth.

Zhang et al. [5] reported the synthesis of β-MnO_2 nanorods and the use as catalysts in the oxidation of methylene blue dye in the presence of H_2O_2. Watts et al. [6] investigated amorphous and crystalline MnO_2 as catalysts for the Fenton-like decomposition of hydrogen peroxide into oxidants and reductants and found the amorphous and crystalline β-MnO_2 at near-neutral pH resulted in significant carbon tetrachloride degradation. Xu et al. [7] investigated the oxidative removal of steroid estrogens from water by MnO_2 and the factors influencing the reactions. MnO_2 exhibited a promising chemical agent under optimized conditions for estrogen removal from water. Dong et al. [8] also evaluated the catalytic properties of β-MnO_2 nanowires for the degradation of phenol and revealed good separability and remarkable catalysis for the degradation of phenol on β-MnO_2 nanowires.

More recently, sulfate radicals have been proposed as an alternative to $OH^•$ for organic oxidation. Production of sulfate radicals can be achieved by heat, light radiation, and metal activation of sulfate oxidants, such as persulfate [9–13] and peroxymonosulfate (PMS) [14–17]. Homogeneous Co^{2+}/PMS system has been found quite effective in sulfate radical production for various organic degradation [14,18–22]. However, Co^{2+} in homogeneous reaction could cause health problem due to the toxicity of Co. Thus, heterogeneous Co/PMS has been a focus. In the past a few years, several investigations have been reported in Co_3O_4 [23,24], supported Co_3O_4 [25–32] and composites [33].

MnO_2 is a common oxide present in soils. It has low toxicity to the environment. As stated above, previous investigation have found that MnO_2 can activate H_2O_2 for $OH^•$ generation. However, no investigation has been reported in MnO_2 activation of

* Corresponding author. Tel.: +61 8 9266 3776; fax: +61 8 9266 2681.
E-mail address: Shaobin.wang@curtin.edu.au (S. Wang).

0926-3373/$ – see front matter © 2012 Elsevier B.V. All rights reserved.
http://dx.doi.org/10.1016/j.apcatb.2012.09.001

peroxymonosulfate. Previously, supported Co_3O_4 have been prepared exclusive using inert supports for PMS activation and the activity strongly depended on supports. In this paper, we report synthesis of a mesoporous MnO_2, its supported Co_3O_4 nanoparticles and their performance in activation of peroxymonosulfate for phenol degradation. We found a synergistic effect of active MnO_2 with Co_3O_4 towards PMS activation and phenol oxidation.

2. Experimental methods

2.1. Material synthesis

A mesoporous MnO_2 samples was prepared by reduction of $KMnO_4$ with maleic acid as reported earlier by Hong et al. [34]. In brief, potassium permanganate was dissolved in distilled water and mixed with a maleic acid solution. The molar ratio of the mixture was $KMnO_4$:Maleic acid = 1:3. The resulting solution was mixed thoroughly and aged for 24 h at room temperature. The brown precipitates were filtered and washed with water several times. The precipitates were dried at room temperature for 24 h and calcined at 300 °C for 4 h at the rate of 3 °C/min. Cobalt oxide (Co_3O_4) was obtained by thermal decomposition of $Co(NO_3)_2$ at 500 °C for 2 h.

Mesoporous MnO_2 supported Co catalysts were prepared by an impregnation method. Typically, the synthesized MnO_2 was mixed with Co precursor solution ($Co(NO_3)_2$) and stirred for 24 h. Then the mixture was put into a rotary evaporator to remove water. After impregnation, the materials were dried and calcined at 500 °C for 4 h. Three MnO_2 supported Co catalysts were prepared with Co loading at 1, 3 and 5 wt%.

2.2. Structure characterization

The particle surface area and pore size measurements were carried out by N_2 adsorption/desorption analysis at −196 °C using a Micromeretics Tristar 3000. Samples were degassed at 200 °C for 24 h prior to adsorption analysis. The surface area and pore size distribution were obtained by the BET and BJH methods, respectively. Temperature programmed reduction (TPR) using H_2 was carried in the range of 50–700 °C using BELCAT. The detail steps of the H_2-TPR were described elsewhere [35].

The crystal structure of the synthesized powders was determined by an X-ray diffractometer (XRD, Bruker D8 Advance) equipped with Cu Kα radiation. The particle morphology was examined from transmission electron microscopy (TEM) obtained using a JEOL JEM1010 electron microscope.

2.3. Catalytic activity tests

Phenol degradation tests were carried out at 30 °C in a 1-L glass vessel with 500 mL of phenol solution at 25 ppm with a constant stirring of 400 rpm. Firstly, 0.05 g catalyst was added into the phenol solution for a while, then oxone ($2KHSO_5{\cdot}KHSO_4{\cdot}K_2SO_4$, PMS, obtained from Aldrich) was added into the solution at 0.5 g/L. At certain time, water sample (1 mL) was withdrawn into a HPLC vial, 0.5 mL of pure methanol was injected into the vial to quench the reaction [27,28]. The concentration of phenol was analyzed using a Varian HPLC with a UV detector set at λ = 270 nm. A C-18 column was used to separate the organics while the mobile phase with a flowrate of 1.5 mL/min was made of 30% CH_3CN and 70% water. For a comparison, a homogeneous oxidation with cobalt ion (Co^{2+}) and oxone was also conducted by addition of the chemicals into the phenol solution simultaneously. The Co^{2+} concentration was kept at the same level as 1 wt%Co loaded on MnO_2.

For selected samples, total organic carbon (TOC) was determined using a Shimadzu TOC-5000 CE analyzer. For the measurement of TOC, 5 mL sample was extracted at a fixed interval and quenched with 5 mL of 3 M sodium nitrite solution and then analyzed on the TOC analyzer [27,28].

For the tests of recycled catalyst, the catalyst was obtained after each run by filtration of reaction solution and thoroughly washing of collected solids with distilled water several times, then drying at 80 °C for 2 h for reuse.

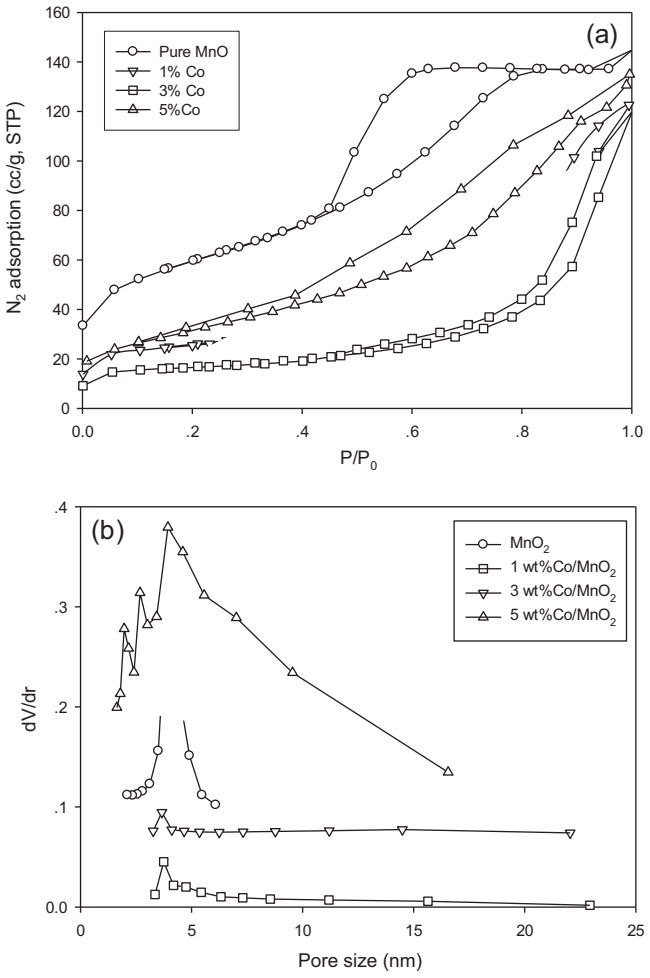

Fig. 1. N_2 adsorption isotherms and pore size distributions of MnO_2 and Co/MnO_2 catalysts. (a) N_2 isotherms and (b) pore size distributions.

3. Results and discussion

Fig. 1 shows N_2 adsorption/desorption isotherm and pore size distribution of MnO_2 and its supported Co catalysts. As can be seen, MnO_2 presented a hysteresis loop at $p/p_0 = 0.5–0.8$, a typical mesopore characteristic. Pore size distribution showed one peak centered at 3.8 nm. Other two catalysts, 1 wt%Co/MnO_2 and 3 wt%Co/MnO_2, show similar N_2 adsorption profiles and pore size distribution with a single peak centered at 3.8 nm. However, 5 wt%Co/MnO_2 showed slight difference in pore size distribution. Apart from the major pore centered at 4 nm, some smaller pores centered at 2.0 and 2.7 nm also appeared, suggesting multiple pore mode of the sample. Surface area ad pore volume of mesoporous MnO_2 and its supported Co catalysts indicated that loading of Co oxide reduced the surface area and pore volume.

Fig. 2 shows XRD patterns of mesoporous MnO_2 and its supported Co catalysts. The synthesized MnO_2 sample presented weak XRD peaks at $2\theta = 12.8°$ and 37.5°, suggesting less crystallinity of this sample. Other three Co/MnO_2 samples showed strong peaks at $2\theta = 12.8°$, 18.1°, 28.6° and 37.5°, which correspond to the

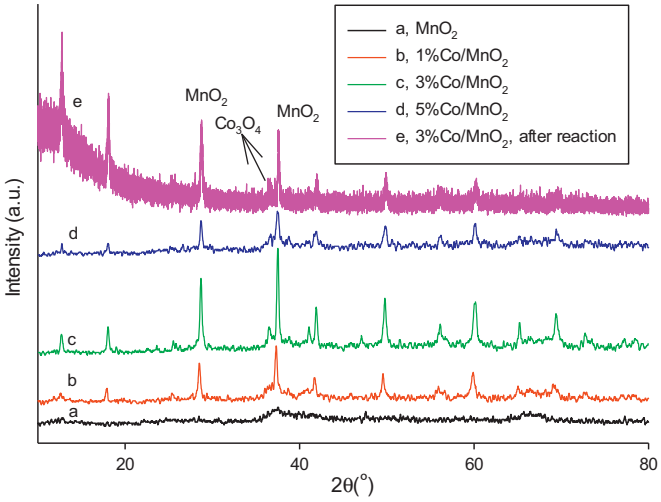

Fig. 2. XRD patterns of MnO_2 and Co/MnO_2 catalysts.

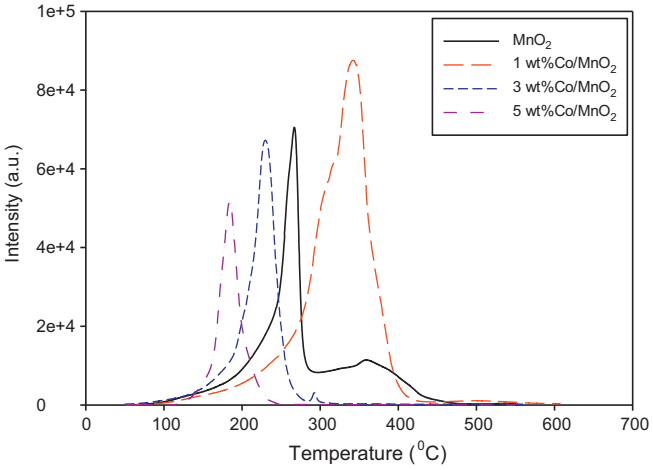

Fig. 4. H_2-TPR profiles of MnO_2 and Co/MnO_2 catalysts.

diffraction of α-MnO_2. Apart from these peaks, a peak at $2\theta = 37.6$ was also identified, which indicates the presence of Co_3O_4 on Co/MnO_2 catalysts.

TEM images (Fig. 3) shows amorphous phase of mesoporous MnO_2 with a well-developed porous structure. However, some changes in MnO_2 phase was observed on 3 wt%Co/MnO_2. TEM image shows amorphous particles and large amount of particles in nanorods with 30 nm in diameter and 50–200 nm in length. The results confirm XRD patterns, demonstrating the phase change from amorphous to crystallinity. Due to the phase change, surface area and pore volume were reduced for Co/MnO_2.

Fig. 4 presents H_2-TPR profiles of MnO_2 and Co/MnO_2 nanoparticles. The TPR pattern of MnO_2 depicts two peaks. A major peak occurred at approximate 270 °C and a small peak at 360 °C, which marks the reduction temperature of MnO_2 to Mn_2O_3 or combined with Mn_3O_4, respectively, indicating the first stage of MnO_2 reduction to Mn_2O_3 followed to Mn_3O_4 at the higher temperature [36]. The catalyst, 1 wt%Co/MnO_2, showed a maximum peak at 340 °C with a shoulder at 315 °C, suggesting the lower reduction of MnO_2 after Co loading. For 3 wt%Co/MnO_2 and 5 wt%Co/MnO_2 catalysts, reduction temperature showed a strong shift to lower temperature at 290 and 190 °C, respectively. TPR results suggest the change of redox potential of MnO_2 and Co/MnO_2 catalysts. For high loading of Co on MnO_2, the redox reaction will occur at low temperature.

Previous investigations have been done on the reducibility of cobalt oxide materials mixed with different kinds of metal oxides by H_2-TPR [37,38]. The reduction profile for Co_3O_4 usually consists of a low-temperature peak below 300 °C and a high-temperature peak between 300 and 700 °C, referring to $Co^{3+} \rightarrow Co^{2+} \rightarrow Co$ processes. Therefore, it is deduced that the strong reduction at low temperature on Co/MnO_2 is due to simultaneous reduction of Co_2O_3 to CoO and MnO_2 to Mn_2O_3.

The degradation of phenol versus time on Co_3O_4, MnO_2, and Co/MnO_2 nanoparticles is illustrated in Fig. 5. A control test for phenol adsorption on MnO_2 without oxone showed 8% reduction in phenol concentration at 180 min, suggesting minor adsorption of phenol on MnO_2 due to low surface area. With the presence of oxone, various catalysts presented different activities in phenol degradation. Co_3O_4 showed a gradual change in phenol degradation. After 180 min, phenol reduction was only about 20%. MnO_2 showed higher initial activity in phenol degradation than Co_3O_4 and the phenol concentration was reduced by 30% in 30 min and continued to decrease but at low rate. At 250 min, phenol degradation was 38%. Co/MnO_2 nanoparticles presented much higher activity than either MnO_2 or Co_3O_4 in phenol degradation. For 1 wt%Co/MnO_2, phenol degradation could reach 97% at 250 min. Other two catalysts, 3 wt%Co/MnO_2 and 5 wt%Co/MnO_2, showed similar phenol degradation efficiency and 100% phenol removal could be obtained at 100 min. TOC measurements indicated that MnO_2 could achieve 45% TOC reduction at 180 min and that Co/MnO_2 catalysts could give similar TOC reduction at 60–70% at 90 min.

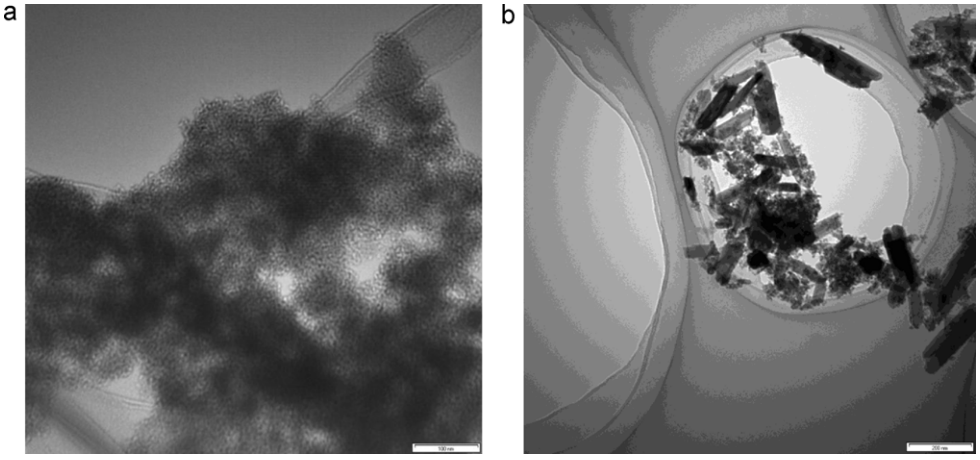

Fig. 3. TEM images of MnO_2 and Co/MnO_2 catalysts. (a) MnO_2 (b) 3 wt%Co/MnO_2.

Table 1
Porous structure of MnO_2 and its supported Co catalysts.

Catalyst	S_{BET} (m^2/g)	V (cm^3/g)	First order kinetics		TOC reduction (%)
			K_1 (min^{-1})	R^2	
MnO_2	179	0.65	–	–	45
1 wt%Co/MnO_2	78	0.25	0.0165 ± 0.0022	0.975	66
3 wt%Co/MnO_2	51	0.23	0.0420 ± 0.0024	0.994	67
5 wt%Co/MnO_2	40	0.32	0.0425 ± 0.0018	0.996	61

After reaction, the solution was checked for leaching using atomic absorption spectroscopy (AAS) and it was found that the concentration of Mn or Co ions is below detection limit, suggesting that leaching did not contribute much to the catalytic activity. The surface area and structure of 3 wt%Co/MnO_2 were also measured by N_2 adsorption and XRD. It was found that S_{BET} and pore volume were 71.9 m^2/g and 0.20 cm^3/g, respectively, which are close to the values of fresh sample. XRD pattern (Fig. 2) of the reacted 3 wt%Co/MnO_2 is also similar to fresh sample, showing Co_3O_4 and MnO_2 peaks. These results suggest that no significant changes occurred for the catalyst during the reaction.

Using a first order kinetic model, $\ln(C/C_0)$ versus time produced straight lines for three MnO_2 supported Co catalysts in phenol degradation as shown in Fig. 6. The parameters are presented in Table 1. Based on regression coefficients, one can see that phenol degradation followed the first order kinetics and rate constants are similar for 3 wt%Co/MnO_2 and 5 wt%Co/MnO_2.

Catalytic tests have shown moderate phenol degradation on Co_3O_4 and MnO_2 in the presence of PMS, suggesting that Co_3O_4 and MnO_2 could activate PMS for sulfate radical production, leading to phenol degradation. The activation reactions could be expressed as below:

$$HSO_5^- + Co_2O_3 \rightarrow SO_5^{2-\bullet} + OH^- + 2CoO \quad (1)$$

$$HSO_5^- + 2CoO \rightarrow SO_4^{2-\bullet} + H^+ + Co_2O_3 \quad (2)$$

$$HSO_5^- + 2MnO_2 \rightarrow SO_5^{2-\bullet} + OH^- + Mn_2O_3 \quad (3)$$

$$HSO_5^- + Mn_2O_3 \rightarrow SO_4^{2-\bullet} + H^+ + 2MnO_2 \quad (4)$$

Co/MnO_2 nanoparticles presented much high phenol degradation than MnO_2 and Co_3O_4, suggesting a synergistic effect of MnO_2 support and Co_3O_4. Due to dispersion of Co_3O_4 on MnO_2, more amounts of active sites (Co_3O_4) were produced on Co/MnO_2 than bulk Co_3O_4. Table 1 shows that BET surface area and pore volume of MnO_2 were higher than Co/MnO_2, thus the activity of MnO_2 and Co/MnO_2 was not well related to porous structure of the catalysts. XRD and TEM show that MnO_2 and Co/MnO_2 present in different crystallinity. Co/MnO_2 presents nanosized crystallites while MnO_2 shows in amorphous state, suggesting that crystallinity of MnO_2 may affect the activity. H_2-TPR profiles of MnO_2 and Co/MnO_2 show a significant decrease in redox temperature on Co/MnO_2 reduction, suggesting much high redox potential for Co/MnO_2. Activation of PMS for sulfate radical generation depends on redox reactions of Co_3O_4 (Eqs. (1) and (2)) and MnO_2 (Eqs. (3) and (4)). Due to high redox potential of Co/MnO_2, sulfate radicals would be produced faster, resulting in much high phenol degradation. HPLC analysis of reacted solutions found the presence of 4-hydroxybenzonic acid, 1,2-dihydroxybenzne, and p-benzoquinone. The concentration variations of the intermediates with time on 3 wt%Co/MnO_2 are shown in Fig. 7. Hydroxylation took place predominantly in the para position since 4-hydroxybenzoic acid and *p*-benzoquinone are the most abundant aromatic intermediates. Therefore, phenol degradation on Co/MnO_2 nanoparticles could be described in Scheme 1.

Fig. 8 further shows the performance of MnO_2 and 1 wt%Co/MnO_2 at higher catalyst and PMS loading in phenol solution. Homogeneous activation of PMS by Co^{2+} for phenol degradation was also presented. One can see that phenol degradation could be significantly enhanced at higher catalyst dosage and PMS concentration. At the conditions of 0.5 g_{cat}/L and 2.0 g_{oxone}/L, phenol conversion could reach 100% at 60 and 20 min on mesoporous MnO_2 and 1 wt%Co/MnO_2, respectively. Meanwhile, phenol degradation in homogeneous Co^{2+}/PMS was 100% at 30 min. Compared with phenol degradation in homogeneous Co^{2+}/PMS, 1 wt%Co/MnO_2 presented better performance in phenol degradation rate and efficiency. Previously, we have investigated several supported Co catalysts, Co/SiO_2 [26], Co/ZSM5 [27], Co/AC [28] and Co/SBA-15 [25] for phenol degradation with PMS. Compared with

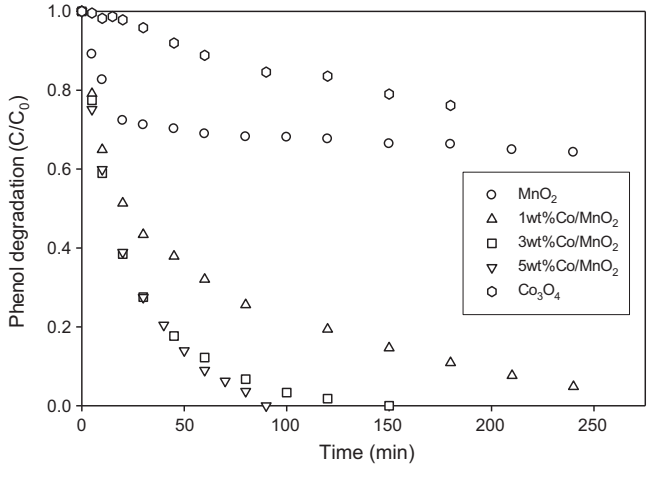

Fig. 5. Phenol degradation on MnO_2 and Co/MnO_2. Reaction conditions: $[phenol]_0$ = 25 ppm, catalyst loading = 0.1 g/L, oxone loading = 0.5 g/L.

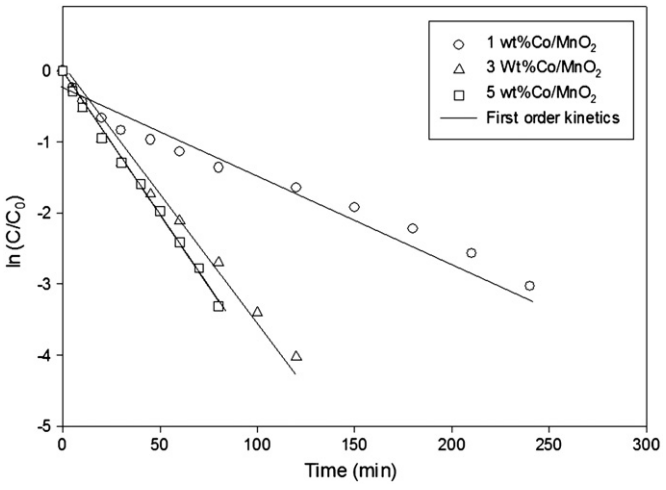

Fig. 6. $Ln(C/C_0)$ versus time in phenol degradation on three Co/MnO_2 catalysts.

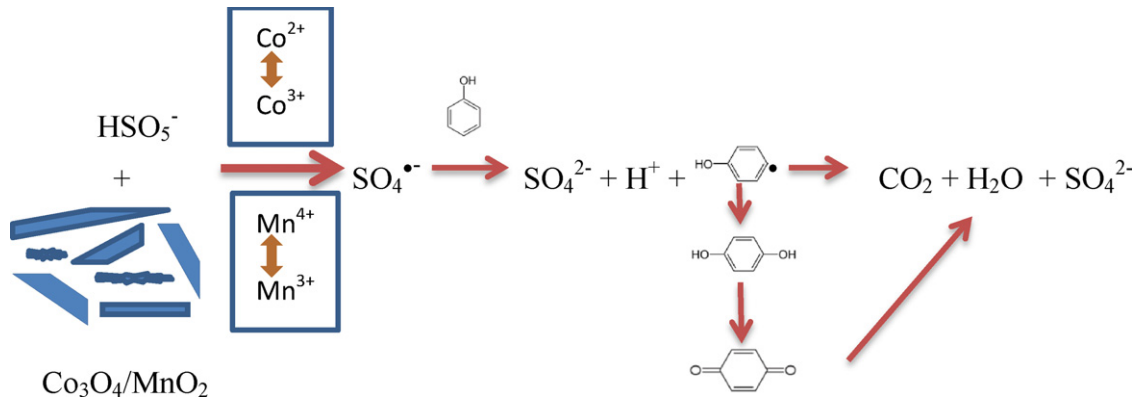

Scheme 1. Co/MnO_2 activation of PMS for phenol degradation.

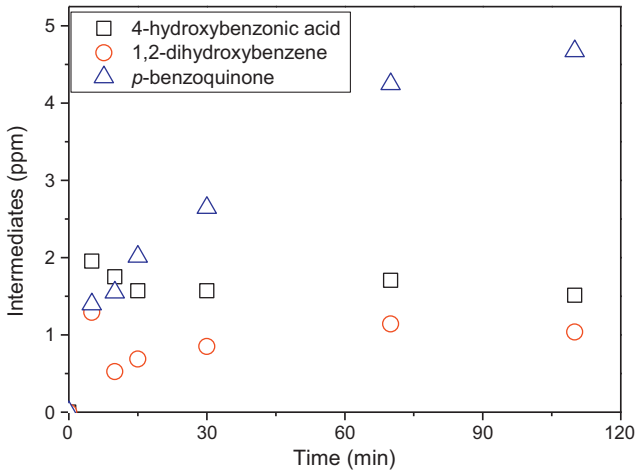

Fig. 7. Variation of intermediate concentrations during phenol degradation on 3 wt%Co/MnO_2.

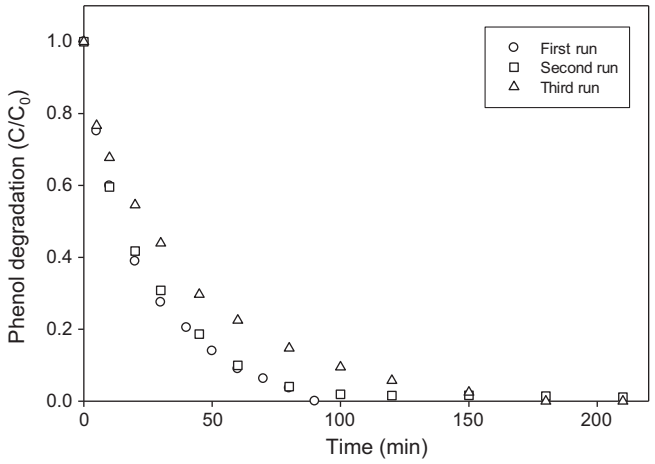

Fig. 9. Stability of 5 wt%Co/MnO_2. Reaction conditions: $[phenol]_0$ = 25 ppm, catalyst loading = 0.1 g/L, oxone loading = 0.5 g/L.

the results, it is also found that Co/MnO_2 exhibited higher activity than the previous supported Co catalysts.

Fig. 9 illustrates the performance of 5 wt%Co/MnO_2 nanoparticles in phenol degradation in three-run tests after the catalyst recycled. As shown, the catalyst presented strong stability in three-run tests. Phenol degradation in the first and second runs was the same and 100% phenol removal could be obtained in 100 min. In the third run, phenol degradation rate showed slight reduction. At 100 min, phenol degradation was 92%. The results indicated that Co/MnO_2 is a promising catalyst with high activity and stability.

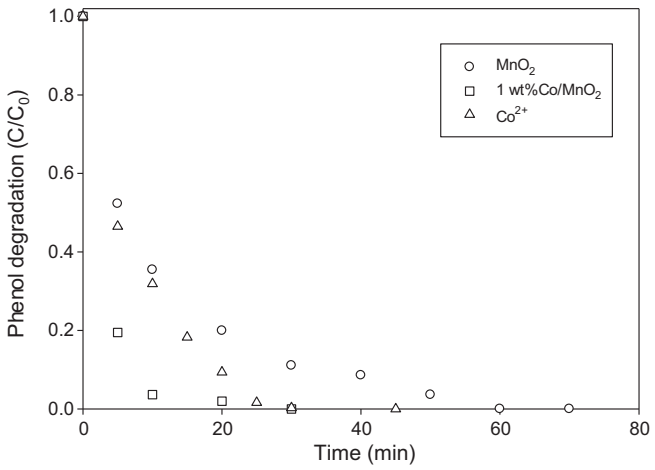

Fig. 8. Phenol degradation on MnO_2 and Co/MnO_2 at varying time. Reaction conditions: $[phenol]_0$ = 25 ppm, catalyst loading = 0.5 g/L, oxone loading = 2.0 g/L.

4. Conclusion

MnO_2 and Co_3O_4 exhibited activity in PMS activation for sulfate radical generation and phenol degradation. Combination of Co_3O_4 and MnO_2 as a catalyst produced a significant synergistic effect in PMS activation and phenol degradation. Co/MnO_2 nanoparticles showed much stronger redox reduction in H_2 at low temperature, making them effective in redox reactions. Co/MnO_2 nanoparticles produced much high activity in PMS activation and phenol degradation could achieve 100% and 60–70% TOC reduction in short time, better performance than Co^{2+}/PMS in homogeneous reaction. Phenol degradation followed the first order kinetics. Co/MnO_2 nanoparticles also demonstrated stable performance in multiple runs, demonstrating as a promising heterogeneous catalyst for organic oxidation.

References

[1] P. Bautista, A.F. Mohedano, J.A. Casas, J.A. Zazo, J.J. Rodriguez, Journal of Chemical Technology and Biotechnology 83 (2008) 1323–1338.
[2] E. Neyens, J. Baeyens, Journal of Hazardous Materials 98 (2003) 33–50.
[3] J.J. Pignatello, E. Oliveros, A. MacKay, Critical Reviews in Environmental Science and Technology 36 (2006) 1–84.
[4] S. Wang, Dyes and Pigments 76 (2008) 714–720.
[5] W. Zhang, Z. Yang, X. Wang, Y. Zhang, X. Wen, S. Yang, Catalysis Communications 7 (2006) 408–412.

[6] R.J. Watts, J. Sarasa, F.J. Loge, A.L. Teel, Journal of Environmental Engineering, ASCE 131 (2005) 158–164.
[7] L. Xu, C. Xu, M.R. Zhao, Y.P. Qiu, G.D. Sheng, Water Research 42 (2008) 5038–5044.
[8] Y.M. Dong, H.X. Yang, K. He, S.Q. Song, A.M. Zhang, Applied Catalysis B: Environmental 85 (2009) 155–161.
[9] C. Liang, C.-F. Huang, Y.-J. Chen, Water Research 42 (2008) 4091–4100.
[10] J. Criquet, N.K.V. Leitner, Chemosphere 77 (2009) 194–200.
[11] V.C. Mora, J.A. Rosso, G. Carrillo Le Roux, D.O. Mártire, M.C. Gonzalez, Chemosphere 75 (2009) 1405–1409.
[12] L. Zhu, J.M. Nicovich, P.H. Wine, Journal of Photochemistry and Photobiology A: Chemistry 157 (2003) 311–319.
[13] S.Y. Yang, P. Wang, X. Yang, L. Shan, W.Y. Zhang, X.T. Shao, R. Niu, Journal of Hazardous Materials 179 (2010) 552–558.
[14] G.P. Anipsitakis, D.D. Dionysiou, Environmental Science & Technology 37 (2003) 4790–4797.
[15] G.P. Anipsitakis, D.D. Dionysiou, Environmental Science & Technology 38 (2004) 3705–3712.
[16] P. Shukla, I. Fatimah, S.B. Wang, H.M. Ang, M.O. Tade, Catalysis Today 157 (2010) 410–414.
[17] P.R. Shukla, S.B. Wang, H.M. Ang, M.O. Tade, Separation and Purification Technology 70 (2010) 338–344.
[18] J. Fernandez, P. Maruthamuthu, A. Renken, J. Kiwi, Applied Catalysis B: Environmental 49 (2004) 207–215.
[19] J. Sun, X. Li, J. Feng, X. Tian, Water Research 43 (2009) 4363–4369.
[20] K.H. Chan, W. Chu, Water Research 43 (2009) 2513–2521.
[21] A. Rastogi, S.R. Al-Abed, D.D. Dionysiou, Water Research 43 (2009) 684–694.
[22] S.K. Ling, S.B. Wang, Y.L. Peng, Journal of Hazardous Materials 178 (2010) 385–389.
[23] G.P. Anipsitakis, E. Stathatos, D.D. Dionysiou, Journal of Physical Chemistry B 109 (2005) 13052–13055.
[24] X.Y. Chen, J.W. Chen, X.L. Qiao, D.G. Wang, X.Y. Cai, Applied Catalysis B: Environmental 80 (2008) 116–121.
[25] P. Shukla, H. Sun, S. Wang, H.M. Ang, M.O. Tadé, Catalysis Today 175 (2011) 380–385.
[26] P. Shukla, H.Q. Sun, S.B. Wang, H.M. Ang, M.O. Tade, Separation and Purification Technology 77 (2011) 230–236.
[27] P. Shukla, S.B. Wang, K. Singh, H.M. Ang, M.O. Tade, Applied Catalysis B: Environmental 99 (2010) 163–169.
[28] P.R. Shukla, S.B. Wang, H.Q. Sun, H.M. Ang, M. Tade, Applied Catalysis B: Environmental 100 (2010) 529–534.
[29] Q. Yang, H. Choi, Y. Chen, D.D. Dionysiou, Applied Catalysis B: Environmental 77 (2008) 300–307.
[30] Q. Yang, H. Choi, D.D. Dionysiou, Applied Catalysis B: Environmental 74 (2007) 170–178.
[31] L.X. Hu, X.P. Yang, S.T. Dang, Applied Catalysis B: Environmental 102 (2011) 19–26.
[32] W. Zhang, H.L. Tay, S.S. Lim, Y.S. Wang, Z.Y. Zhong, R. Xu, Applied Catalysis B: Environmental 95 (2010) 93–99.
[33] Q. Yang, H. Choi, S.R. Al-Abed, D.D. Dionysiou, Applied Catalysis B: Environmental 88 (2009) 462–469.
[34] X.L. Hong, G.Y. Zhang, H.Q. Yang, Y.Y. Zhu, Journal of Materials Synthesis and Processing 10 (2002) 297–302.
[35] A. Patel, P. Shukla, T. Rufford, S. Wang, J. Chen, V. Rudolph, Z. Zhu, Applied Catalysis A: General 409–410 (2011) 55–65.
[36] W. Tian, H. Yang, X. Fan, X. Zhang, Journal of Hazardous Materials 188 (2010) 105–109.
[37] H.-Y. Lin, Y.-W. Chen, Materials Chemistry and Physics 85 (2004) 171–175.
[38] H. Yoshino, C. Ohnishi, S. Hosokawa, K. Wada, M. Inoue, Journal of Materials Science 46 (2011) 797–805.